Supplemental Material to Process dependence of Climate Carbon-cycle feedbacks in UKESM1.1

Spencer K. Liddicoat[1,2*], Chris D. Jones[1,3], Lina M. Mercado[2,4], Eddy Robertson[1], Stephen Sitch[2] and Andy Wiltshire[1,2]

[1]Met Office, FitzRoy Road, Exeter, Devon, EX1 3PB, UK
[2]Faculty of Environment, Science and Economy, University of Exeter, North Park Road, Exeter, EX4 4QE, UK
[3]Cabot Institute for the Environment, University of Bristol, BS8 1UH, UK
[4]UK CEH Centre for Ecology and Hydrology, Wallingford, UK

*Corresponding author. Email: spencer.liddicoat@metoffice.gov.uk

Description of UKESM1.1

All experiments were performed using variants of UKESM1.1 (Mulcahy et al., 2023), which is an updated version of UKESM1-0-LL (Sellar et al. 2019). UKESM1-0-LL performed the majority of the simulations which provided the Met Office and UK NERC partners contribution to CMIP6, and is included in many multi-model carbon cycle-related publications released since then (Arora et al., 2020, Liddicoat et al., 2021, Hajima et al., 2025, Loughlan et al., 2023). UKESM1.1 is an intermediary between UKESM1-0-LL and UKESM2.0 which is under development for use in CMIP7.

UKESM1.1 addresses some of the biases of UKSM1-0-LL; most importantly, UKESM1-0-LL exhibited a cold bias in global mean temperature of almost 0.5°C in the late 20th century (Sellar et al., 2019). This was found to be due to overly strong aerosol forcing resulting from a high bias in SO_2, a precursor to sulphate aerosol, above regions of high anthropogenic emissions. Improved dry deposition of sulphate in UKESM1.1 led to a significant reduction in the cold bias observed in UKESM1-0-LL (Hardacre et al., 2021). In addition, several less significant improvements and bug fixes have been implemented in UKESM1.1. Although using UKESM1-0-LL as the basis for these experiments would facilitate direct comparison with the results of the model as described in the feedback analysis of Arora et al. (2020), the bias correction and bug fixes described above make UKESM1.1 the optimal choice for the present study.

UKESM1.1 is structurally identical to UKESM1-0-LL, described in detail in Sellar et al. (2019). The atmosphere component is version 12.0 of the Met Office Unified Model (UM), with a resolution of 1.25° latitude x 1.875° longitude with top of atmosphere at 85km. Embedded in the atmosphere is the UKCA model (UK Chemistry and Aerosols, Archibald et al. 2020) which determines atmospheric composition through simulation of atmospheric chemistry and aerosol processes. The UM is coupled to the NEMO (Nucleus for European Modelling of the Ocean, Storkey et al., 2018) ocean model. The ocean carbon cycle is represented by inclusion of the ocean biogeochemistry model, MEDUSA (Model of Ecosystem Dynamics, nutrient Utilisation, Sequestration and Acidification; Yool et al. 2013).

The land component of UKESM1.1, vn6.1 of JULES (Joint UK Land Environment Simulator, Clark et al., 2011) is of most relevance to the experiments presented here, their focus being land carbon cycle processes; a brief summary of the carbon cycle elements of JULES now follows.

JULES permits dynamic vegetation in response to changing climate through inclusion of the TRIFFID dynamic vegetation model (Top Down Representation of Interactive Foliage and Flora Including Dynamics, Cox, 2001) which simulates height-based competition between 9 natural plant functional types (PFTs) and, separated from the natural PFTs, two crop and pasture PFTs. The natural PFTs are subject to nutrient (nitrogen) limitation; the potential net primary production (NPP) has an associated nitrogen requirement and is reduced accordingly if this requirement cannot be met by the available nitrogen, with the excess NPP, unassimilable by the vegetation, forming a diagnostic exudates term.

The vegetation emits biogenic volatile organic compounds (BVOCs), isoprene, terpene, acetone and methanol; in standard UKESM1.1 these are passed to UKCA leading to many changes in atmospheric composition, including a reduction in methane lifetime, greater secondary organic aerosol and cloud condensation nuclei load and an increase in ozone. In the control configuration, these are prescribed however, as one of the experimental configurations includes interactive BVOCs.

Below ground carbon is stored in four soil carbon pools each with its own characteristic decay rate. There is no explicit litter pool, but a vegetation-to-soil litter flux is simulated, with litter entering the Decomposable Plant Material (DPM) and Resistant Plant Material (RPM) pools at a proportion dependent upon the nature of the originating PFT. As the carbon in these pools decays, which proceeds much more slowly in the RPM than the DPM pool, some forms a carbon flux to the atmosphere (diagnostic only in CO_2 concentration-driven mode), while the rest is passed to the

Biomass (BIO) and Humified Organic Matter (HUM) soil carbon pools; the HUM pool has the longest turnover time of the four pools.

Associated with each soil carbon pool is an equivalent nitrogen pool, of which there is a fifth, inorganic nitrogen, pool. The overlying vegetation has access to the inorganic nitrogen pool; the different PFTs all access the one inorganic nitrogen pool, which is replenished through the decay of organic matter in the BIO and HUM pools as well as via an atmospheric nitrogen deposition flux, which is prescribed, and bacterial nitrogen fixation as a function of NPP.

References

Archibald, A. T., O'Connor, F. M., Abraham, N. L., ArcherNicholls, S., Chipperfield, M. P., Dalvi, M., Folberth, and co-authors, 2020: Description and evaluation of the UKCA stratosphere–troposphere chemistry scheme (StratTrop vn 1.0) implemented in UKESM1, *Geosci. Model Dev.*, **13**, 1223–1266, https://doi.org/10.5194/gmd-13-1223-2020

Arora V. K., Katavouta A., Williams R. G., Jones C. D., Brovkin V., Friedlingstein P., Schwinger J., Bopp L., Boucher O., Cadule P., 2020: Carbon–concentration and carbon–climate feedbacks in CMIP6 models and their comparison to CMIP5 models, *Biogeosciences*, **17**, 4173–4222, https://doi.org/10.5194/bg-17-4173-2020

Clark, D. B., Mercado, L. M., Sitch, S., Jones, C. D., Gedney, N., Best, M. J., Pryor, M., Rooney, G. G., Essery, R. L. H., Blyth, E., Boucher, O., Harding, R. J., Huntingford, C., and Cox, P. M., 2011: The Joint UK Land Environment Simulator (JULES), model description – Part 2: Carbon fluxes and vegetation dynamics, *Geosci. Model Dev.*, **4**, 701–722, https://doi.org/10.5194/gmd-4- 701-2011

Cox, P. M., 2001: Description of the "TRIFFID" dynamic global vegetation model, Hadley Centre Technical Note, Met Office Hadley Centre, Exeter, Devon, United Kingdom.

Hajima, T., Tachiiri, K., Ito, A., and Kawamiya, M., 2014: Uncertainty of Concentration–Terrestrial Carbon Feedback in Earth System Models, *J. Clim.*, **27**, 3425–3445, https://doi.org/10.1175/JCLI-D-13-00177.1.

Liddicoat, S. K. Wiltshire, A. J., Jones, C. D., et al., 2021: Compatible Fossil Fuel CO_2 Emissions in the CMIP6 Earth System Models' Historical and Shared Socioeconomic Pathway Experiments of the Twenty-First Century. *J. Climate*, **34**, 2853–2875, https://doi.org/10.1175/JCLI-D-19-0991.1.

Loughran, T. F., Ziehn, T., Law, R., Canadell, J. G., Pongratz, J., Liddicoat, S., et al., 2023: Limited mitigation potential of forestation under a high emissions scenario: Results from multi-model and single model ensembles. *J. Geophys. Res. Biogeosciences*, **128**, https://doi.org/10.1029/2023JG007605

Mulcahy, J. P. and Jones, C. G. and Rumbold, S. T. and co-authors, 2023: UKESM1.1: development and evaluation of an updated configuration of the UK Earth System Model, *Geoscientific Model Development*, **16(6)**, https://gmd.copernicus.org/articles/16/1569/2023/10.5194/gmd-16-8041569-2023

Sellar, A. A., Jones, C. G., Mulcahy, J. P., Tang, Y., Yool, A., Wiltshire, A., et al., 2019: UKESM1: Description and evaluation of the U.K. Earth System Model, *J. Adv, Model, Earth Syst.*, **11**, 4513–4558, https://doi.org/10.1029/2019MS001739

Storkey, D., Blaker, A. T., Mathiot, P., Megann, A., Aksenov, Y., Blockley, E. W., Calvert, D., Graham, T., Hewitt, H. T., Hyder, P., Kuhlbrodt, T., Rae, J. G. L., Sinha, B. (2018). UK Global Ocean GO6 and GO7: a traceable hierarchy of model resolutions. *Geoscientific Model Development*, **11(8)**, 3187–3213. https://doi.org/10.5194/gmd-11-3187-2018

Yool, A., Popova, E. E., Anderson, T. R., 2013: MEDUSA-2.0: an intermediate complexity biogeochemical model of the marine carbon cycle for climate change and ocean acidification studies. *Geosci. Model Dev.*, **6(5)**, 1767–1811. https://doi.org/10.5194/gmd-6-1767-2013

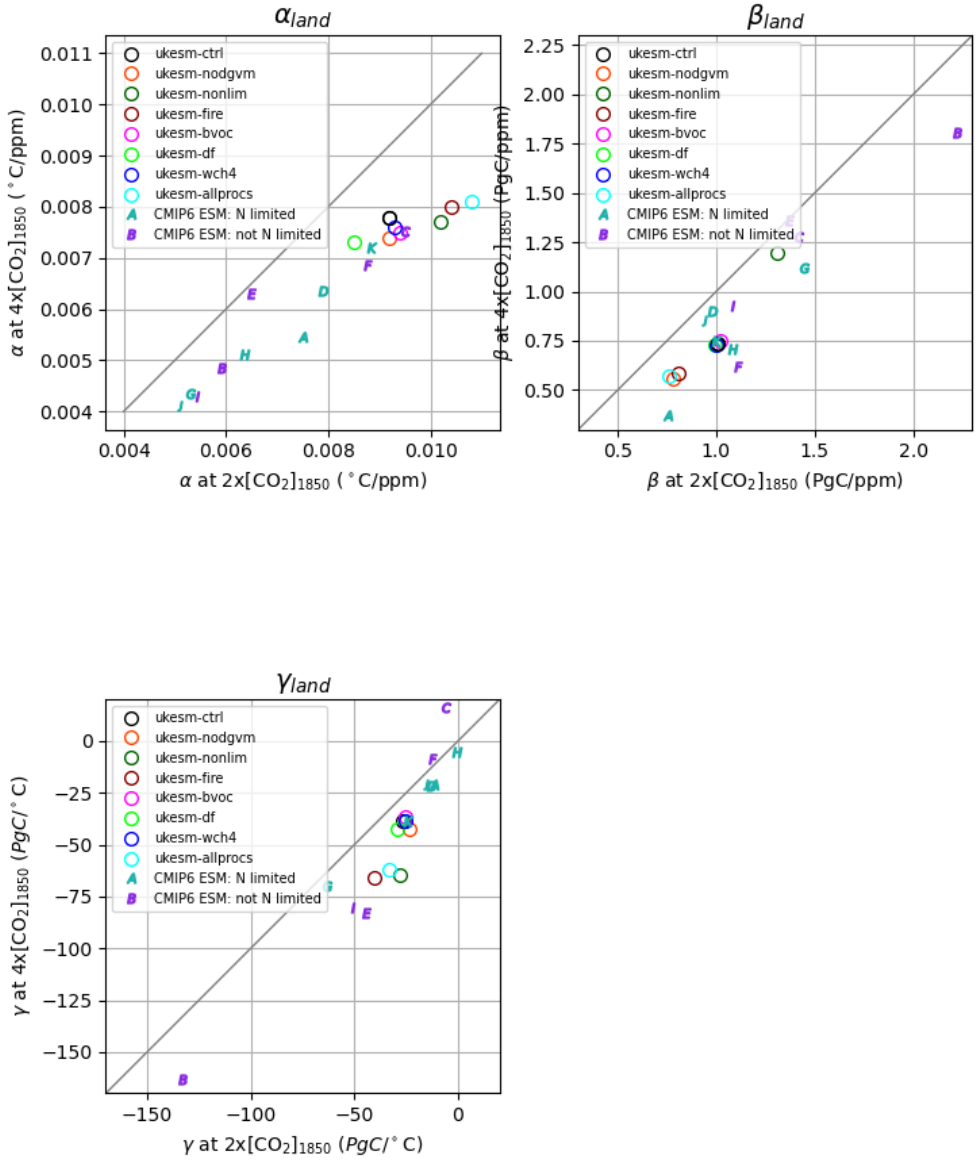

Figure S1: a) Transient climate sensitivity, α, b) carbon-concentration feedback parameter, β, over land, and c) carbon-climate feedback parameter, γ, over land at 4x (y-axis) versus 2x (x-axis) pre-industrial atmospheric CO_2 for the 8 configurations of the UKESM process-ensemble (coloured circles) and for 11 CMIP6 ESMs, lettered. Letters correspond to ESMs as follows: A) ACCESS-ESM-1.5, B) BCC-CSM2-MR, C) CanESM5, D) CESM2, E) CNRM-ESM2-1, F) IPSL-CMS6-LR, G) MIROC-ES2L, H) MPI-ESM1.2-LR, I) GFDL-ESM4, J) NorESM2-LM, K) UKESM1-0-LL.

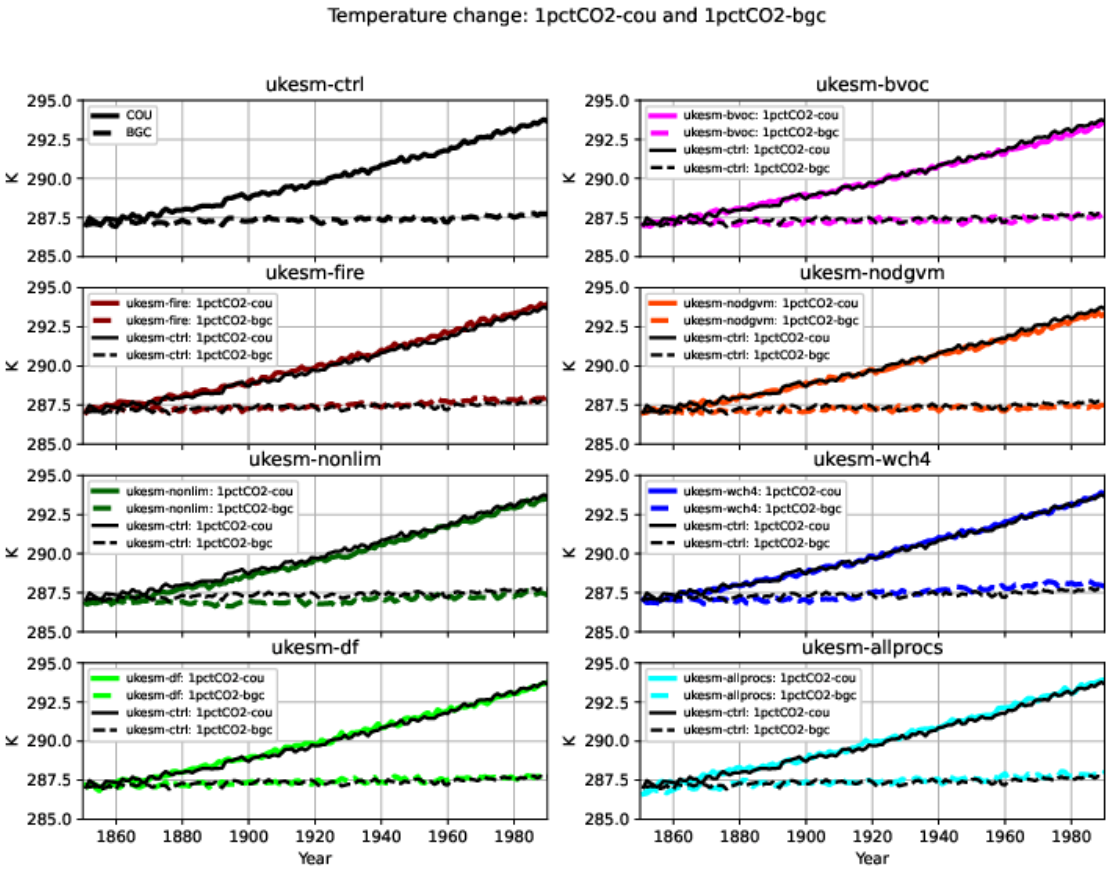

Figure S2: Timeseries of global mean temperature in the *1pctCO2-cou* and *1pctCO2-bgc* experiments of each configuration of the UKESM ensemble: a) *ukesm-ctrl* b) *ukesm-bvoc* c) *ukesm-fire* d) *ukesm-nodgvm* e) *ukesm-nonlim* f) *ukesm-wch4* g) *ukesm-df* h) *ukesm-allprocs* . In each of the experimental configurations, *ukesm-ctrl* is included for comparison.

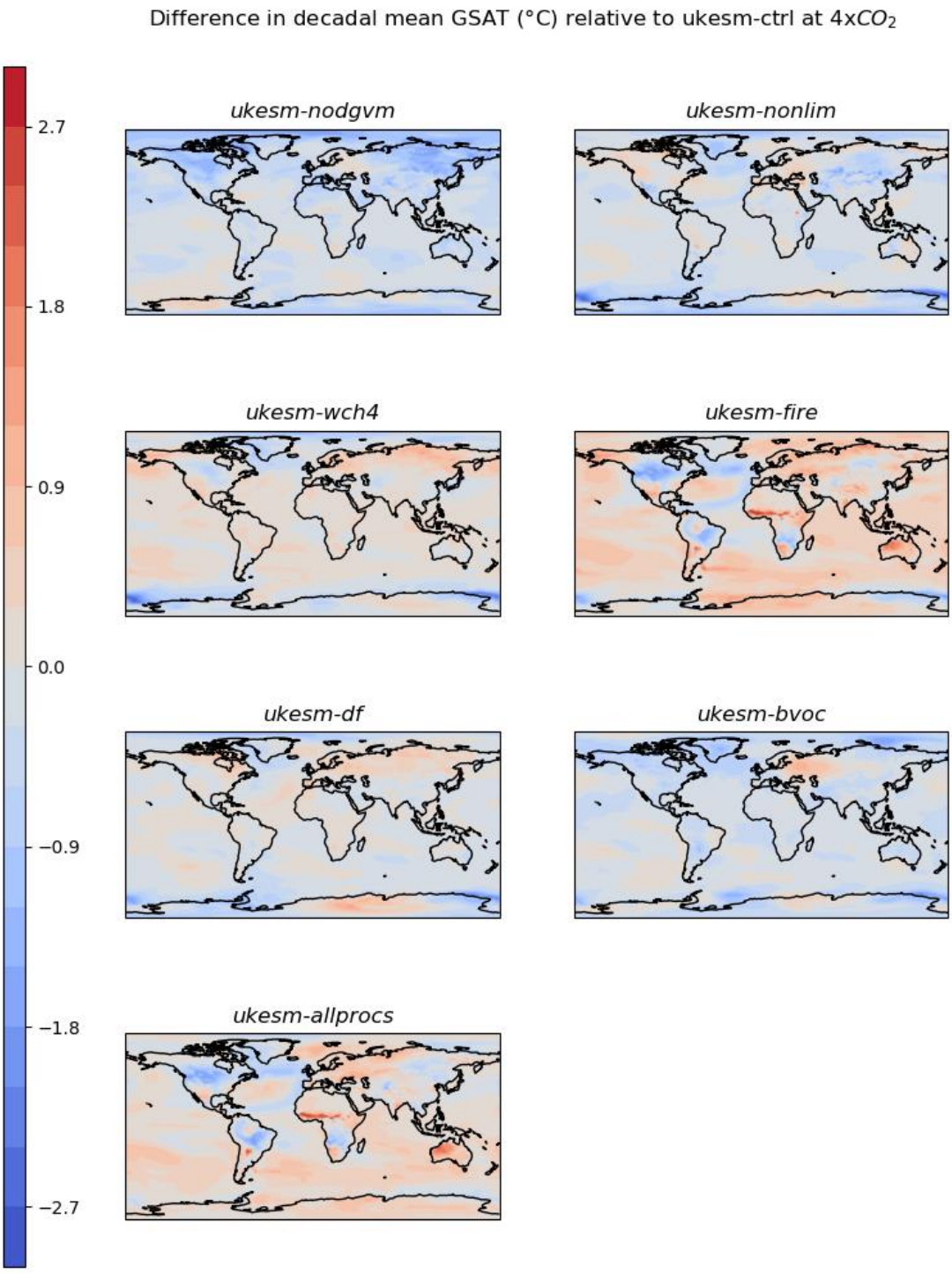

Figure S3: Difference in decadal mean global mean surface air temperature centred on 1990 at 4xCO_2 in each experimental configuration relative to the *ukesm-ctrl.*

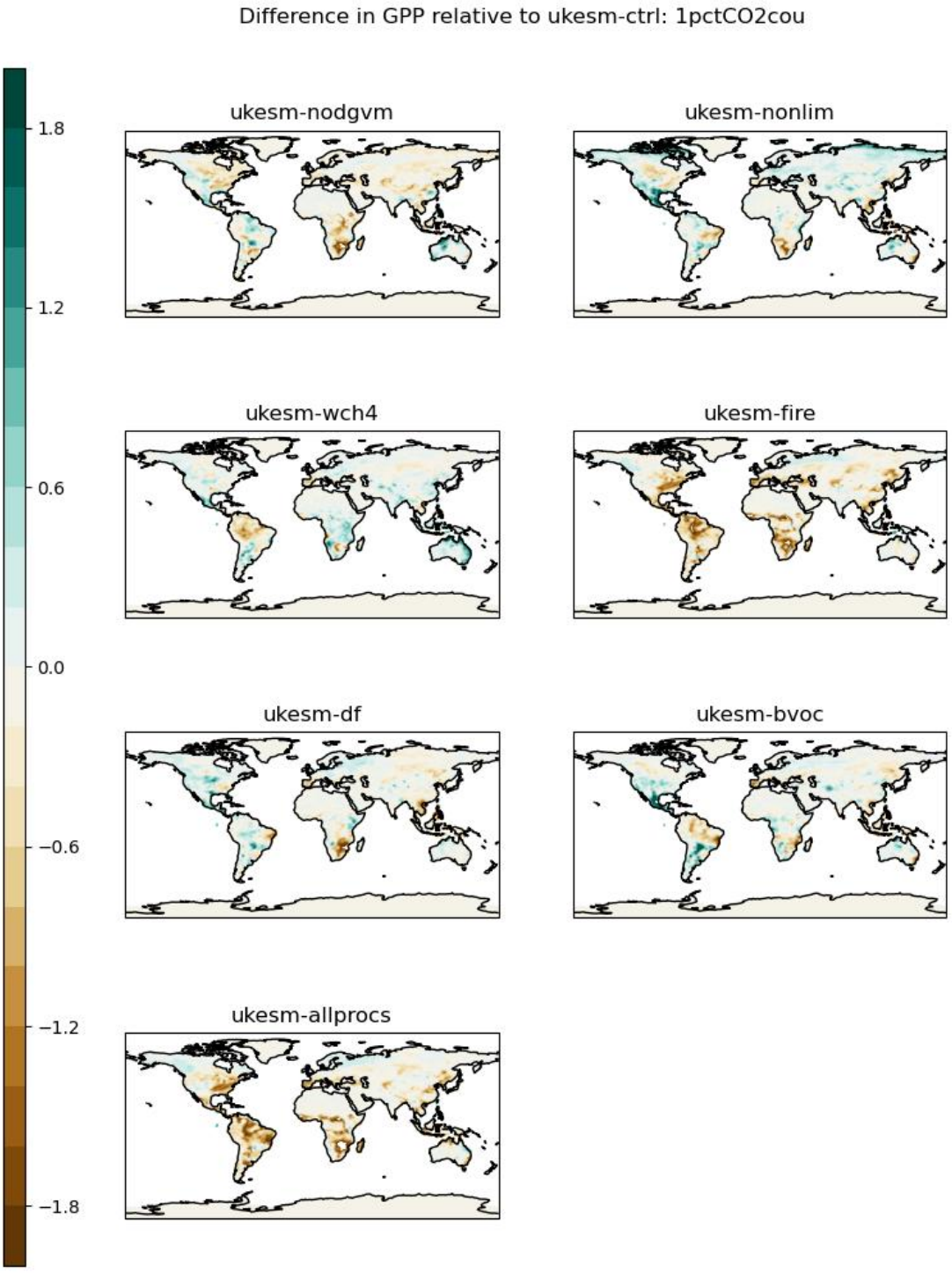

Figure S4: Difference in gross primary production relative to *ukesm-ctrl* for year 1990 of the 1pctCO2-cou simulation by each experimental configuration of UKESM1.1.

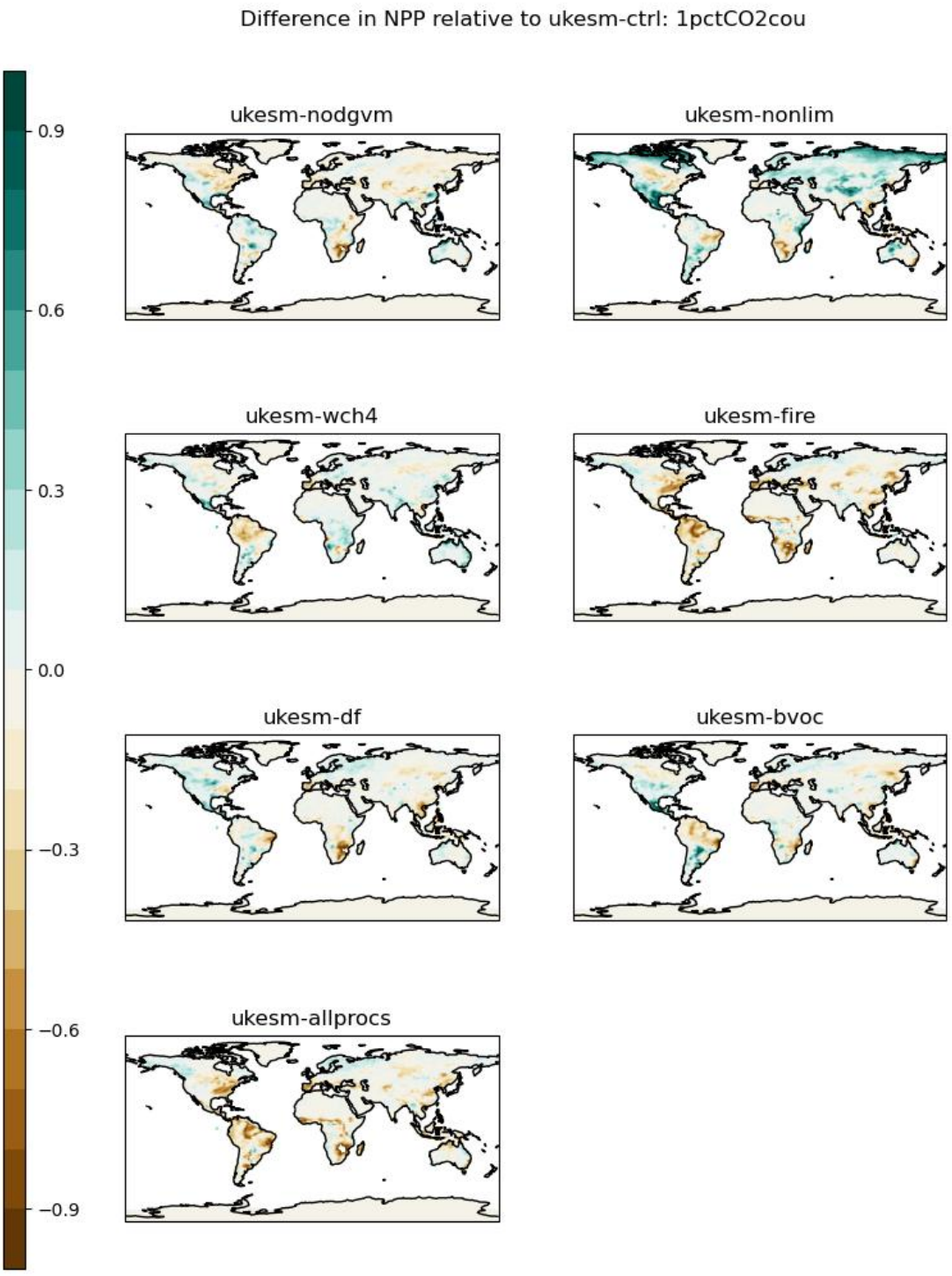

Figure S5: Difference in net primary production relative to *ukesm-ctrl* for year 1990 of the 1pctCO2-cou simulation by each experimental configuration of UKESM1.1.

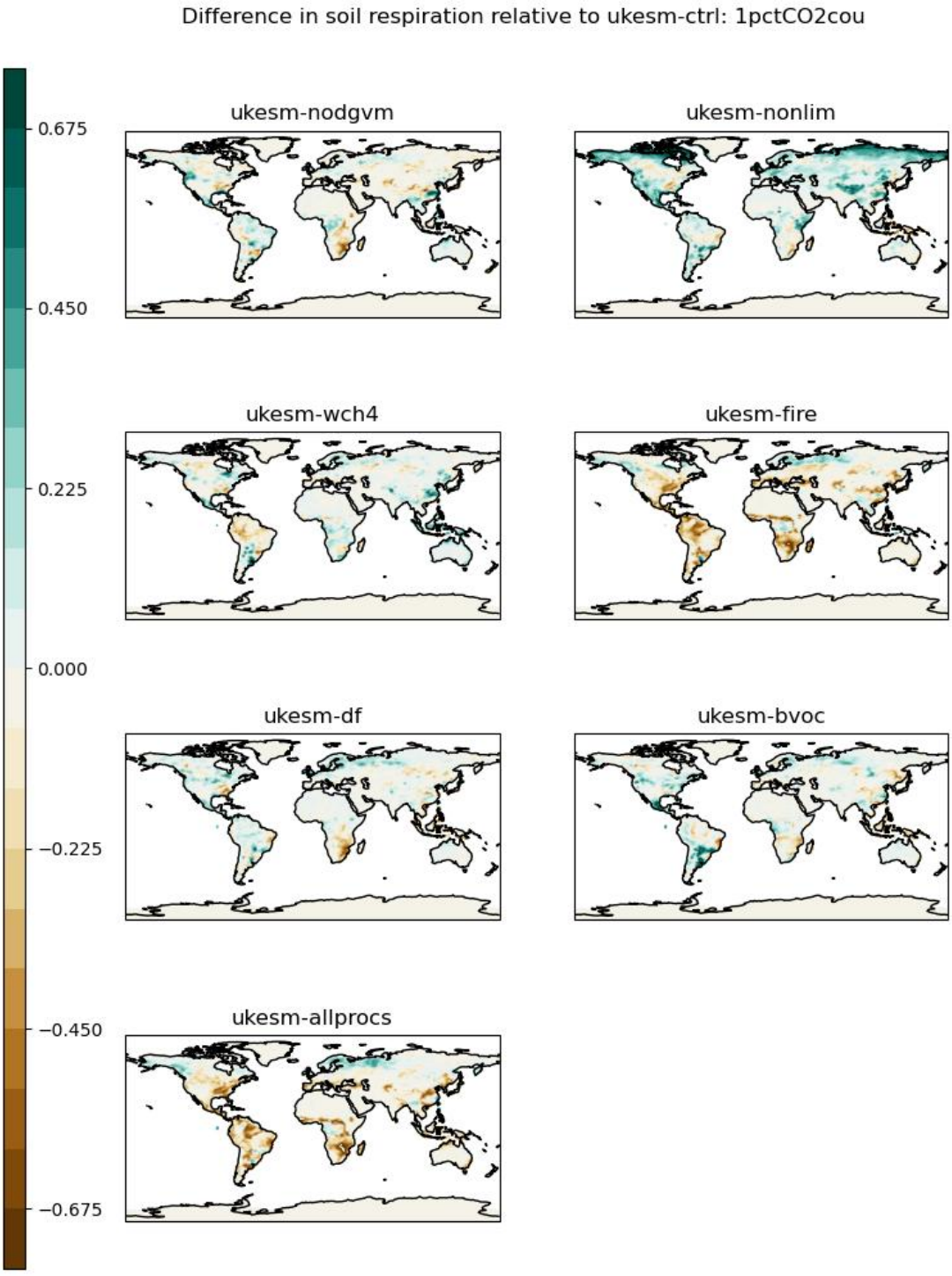

Figure S6: Difference in soil respiration relative to *ukesm-ctrl* for year 1990 of the 1pctCO2-cou simulation by each experimental configuration of UKESM1.1.

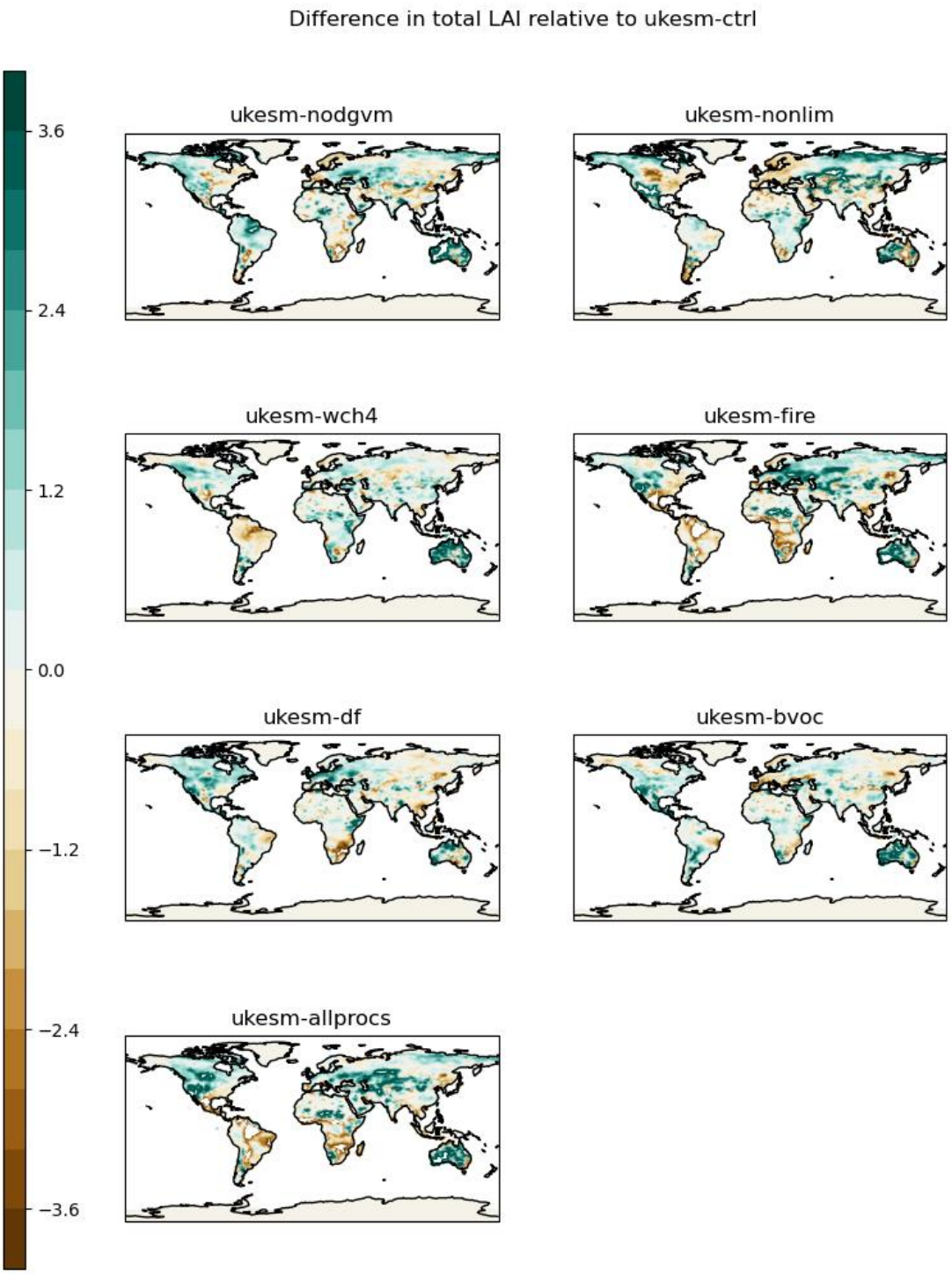

Figure S7: Difference in leaf area index relative to *ukesm-ctrl* for year 1990 of the 1pctCO2-cou simulation by each experimental configuration of UKESM1.1.

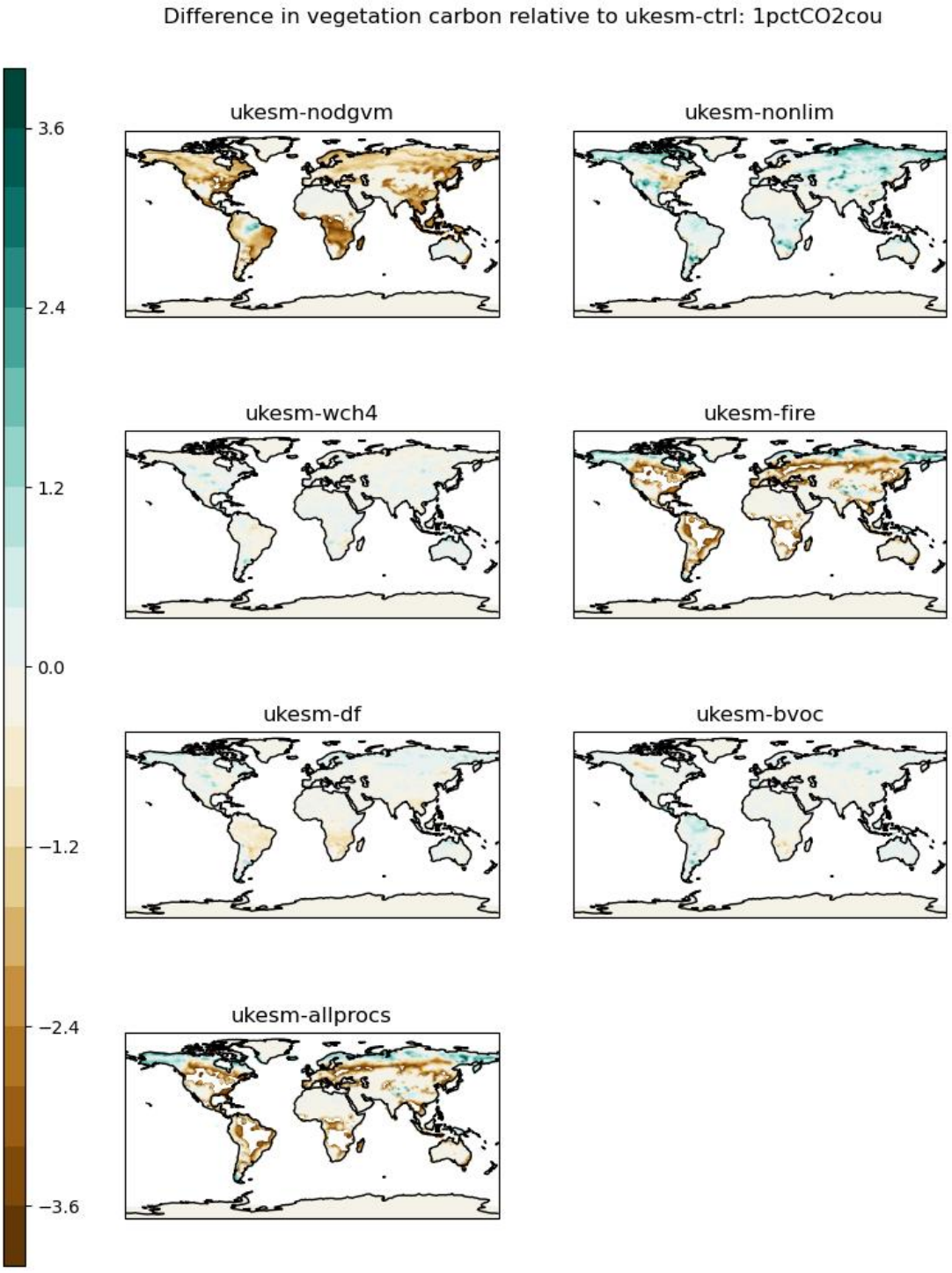

Figure S8: Difference in vegetation carbon relative to *ukesm-ctrl* for year 1990 of the 1pctCO2-cou simulation by each experimental configuration of UKESM1.1

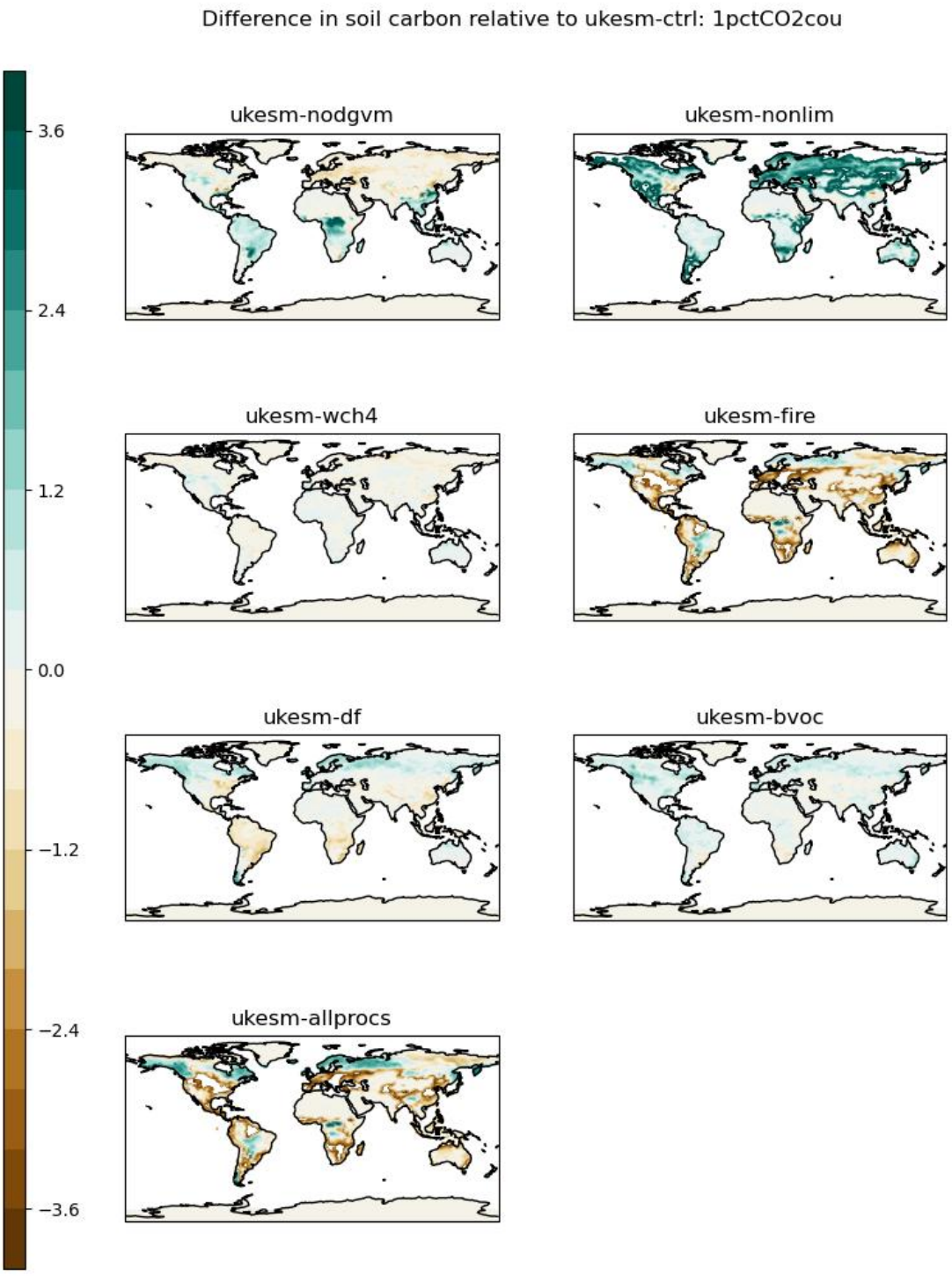

Figure S9: Difference in soil carbon relative to *ukesm-ctrl* for year 1990 of the 1pctCO2-cou simulation by each experimental configuration of UKESM1.1.

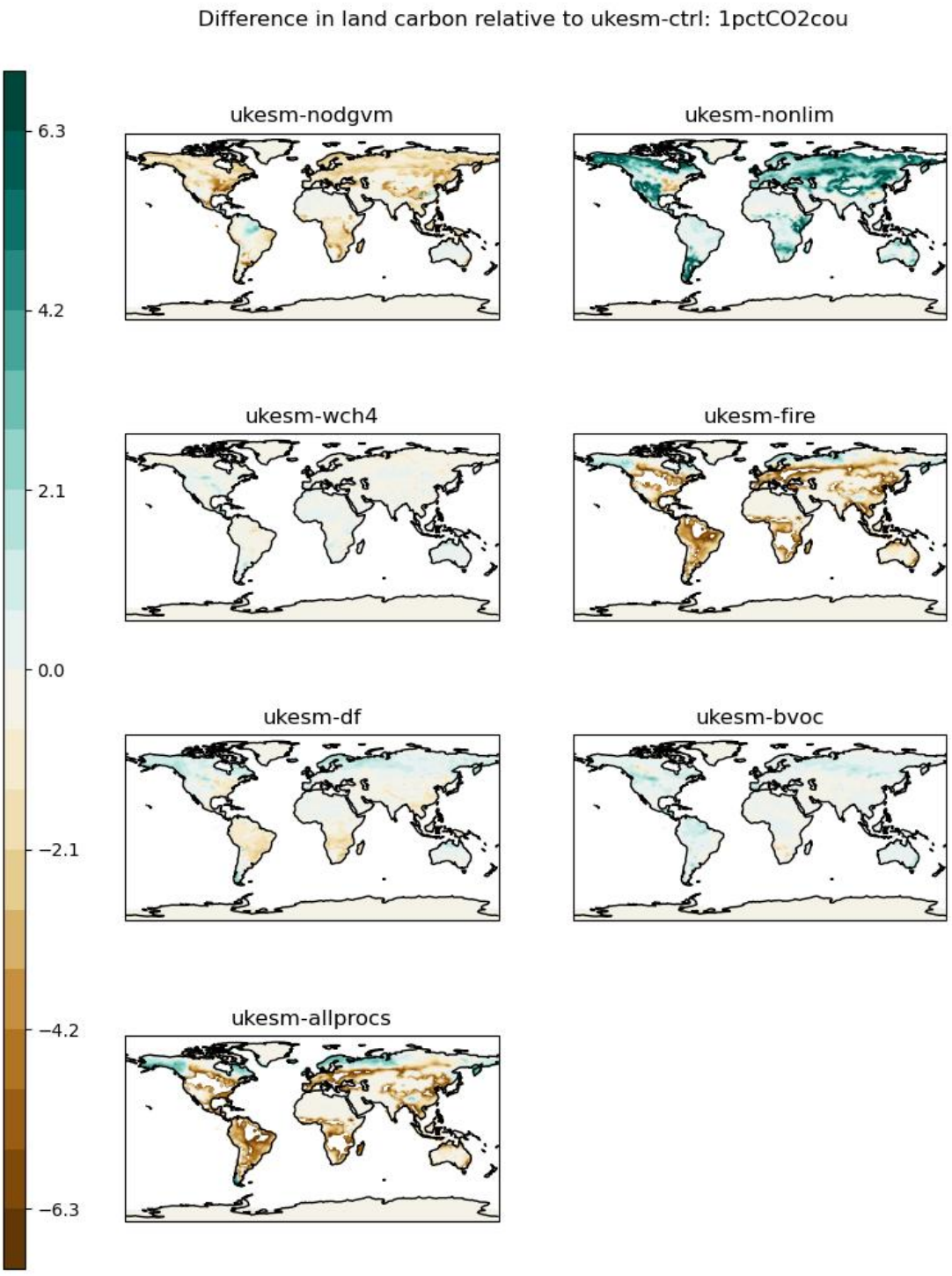

Figure S10: Difference in land carbon store relative to *ukesm-ctrl* for year 1990 of the 1pctCO2-cou simulation by each experimental configuration of UKESM1.1.

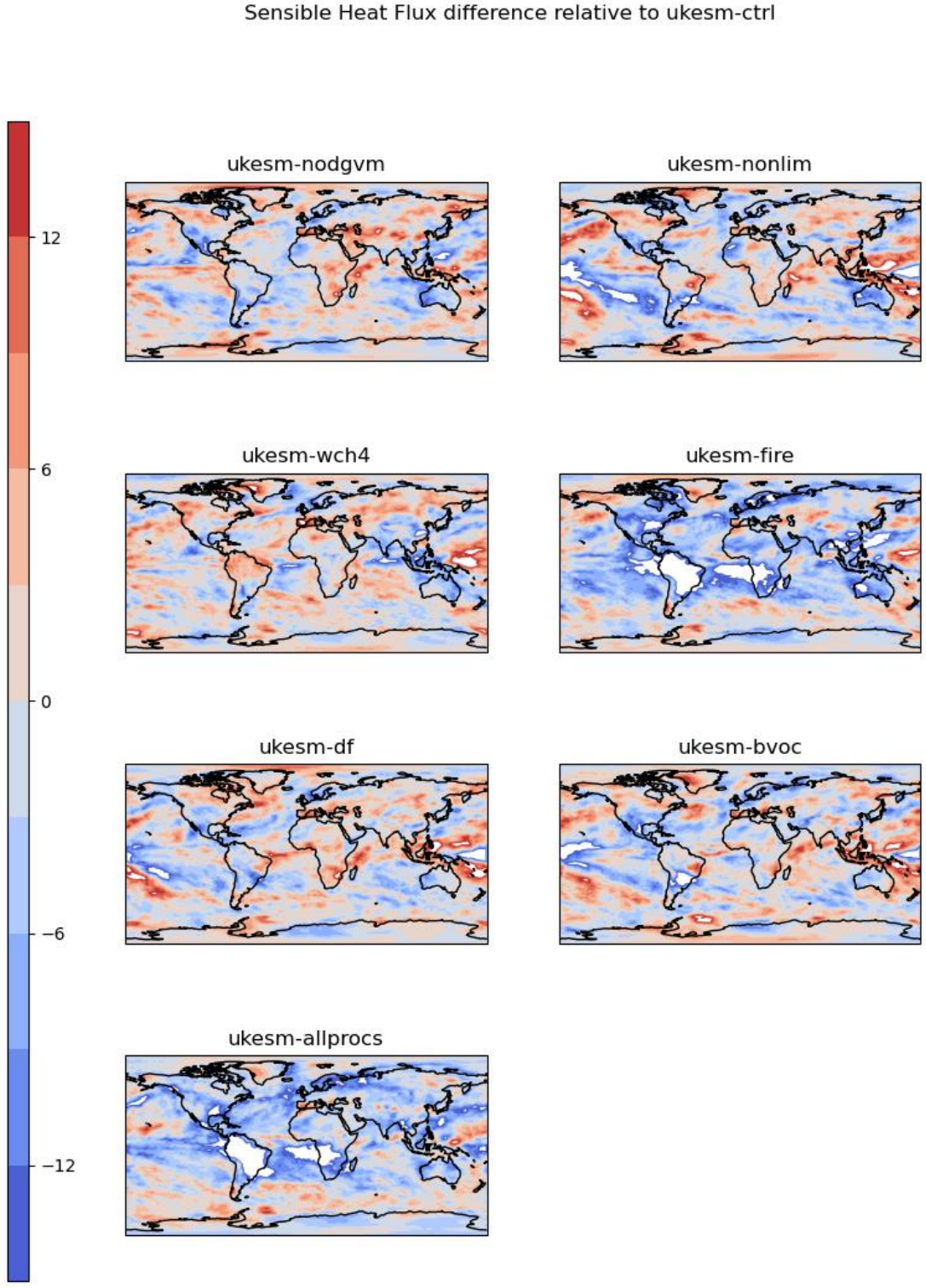

Figure S11: Difference in sensible heat flux (W/m2) relative to *ukesm-ctrl* for year 1990 of the 1pctCO2-cou simulation by each experimental configuration of UKESM1.1.

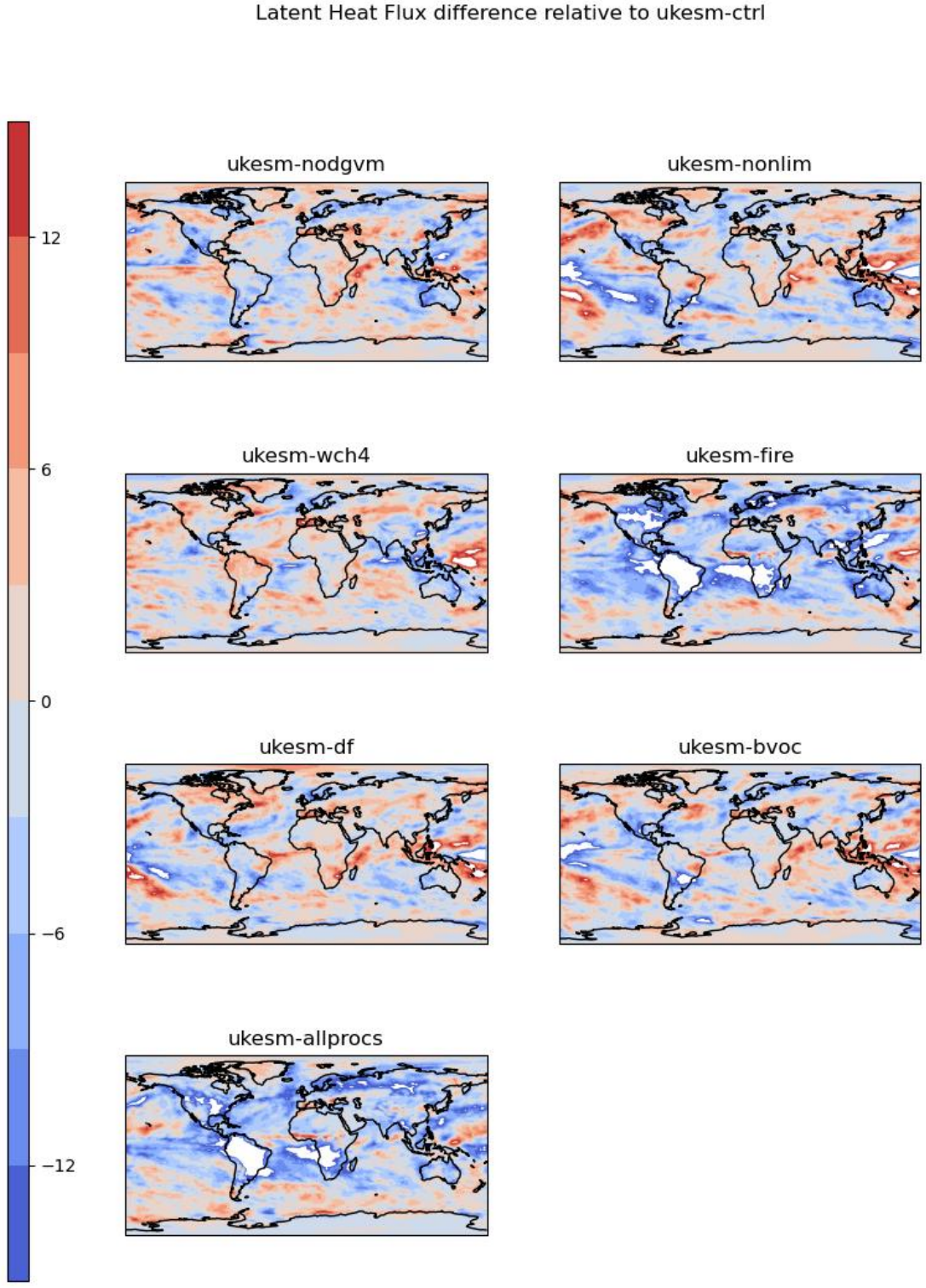

Figure S12: Difference in latent heat flux (W/m2) relative to *ukesm-ctrl* for year 1990 of the 1pctCO2-cou simulation by each experimental configuration of UKESM1.1.

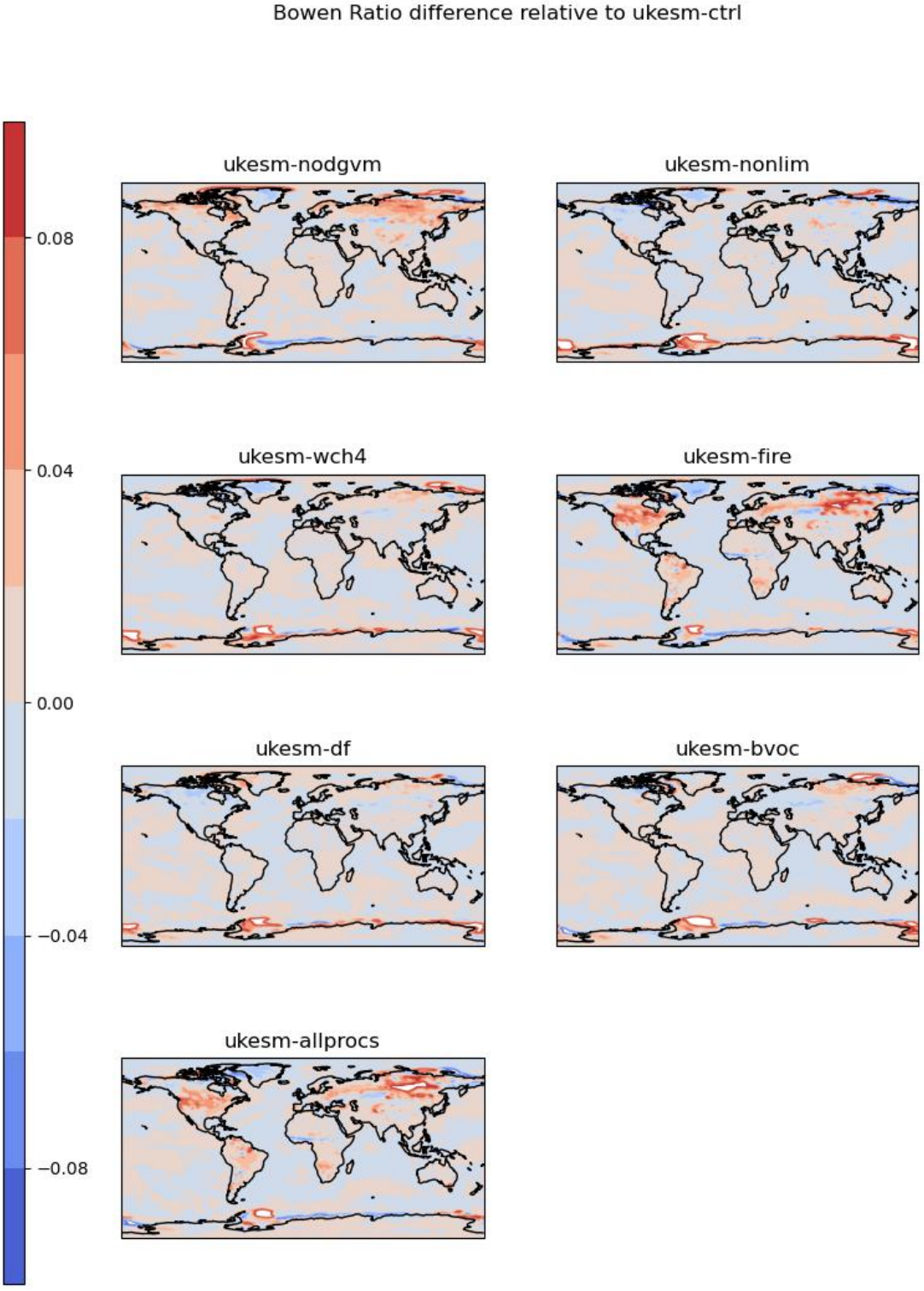

Figure S13: Difference in Bowen Ration (ratio of sensible heat flux to latent heat flux) relative to *ukesm-ctrl* for year 1990 of the 1pctCO2-cou simulation by each experimental configuration of UKESM1.1.

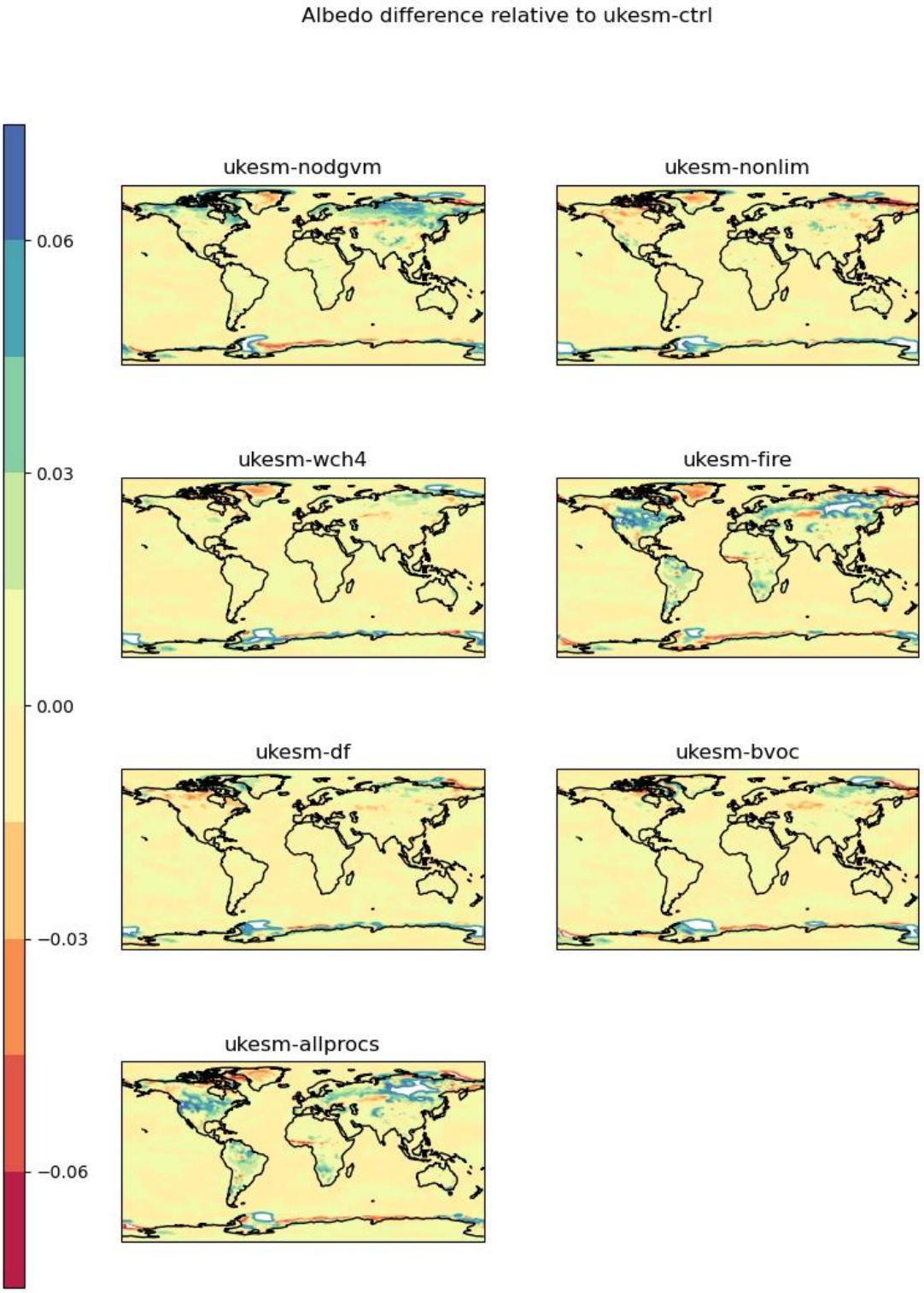

Figure S14: Difference in albedo relative to *ukesm-ctrl* for year 1990 of the 1pctCO2-cou simulation for each experimental configuration of UKESM1.1.

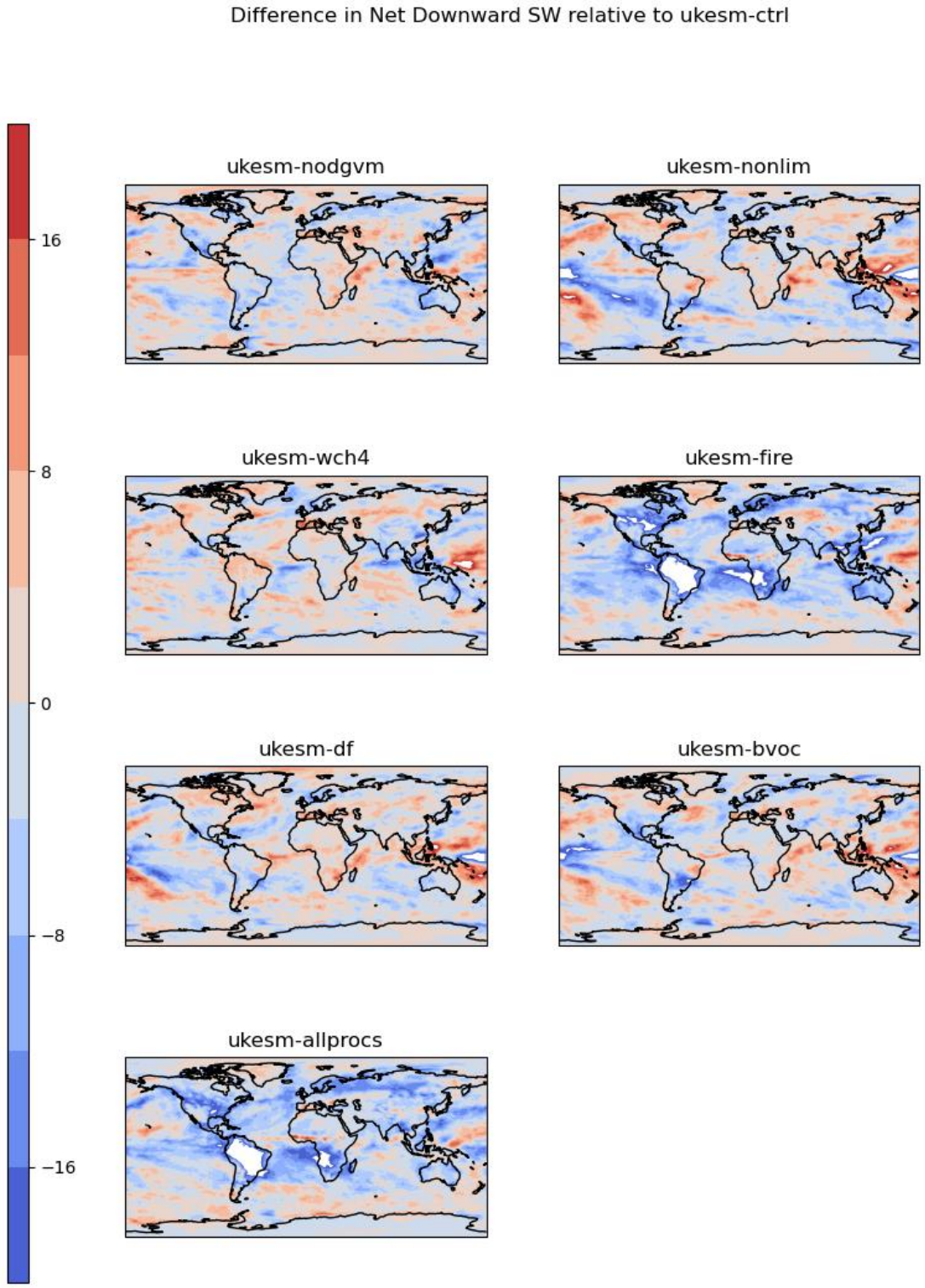

Figure S15: Difference in net downward shortwave radiation (W/m2) relative to *ukesm-ctrl* for year 1990 of the 1pctCO2-cou simulation by each experimental configuration of UKESM1.1.

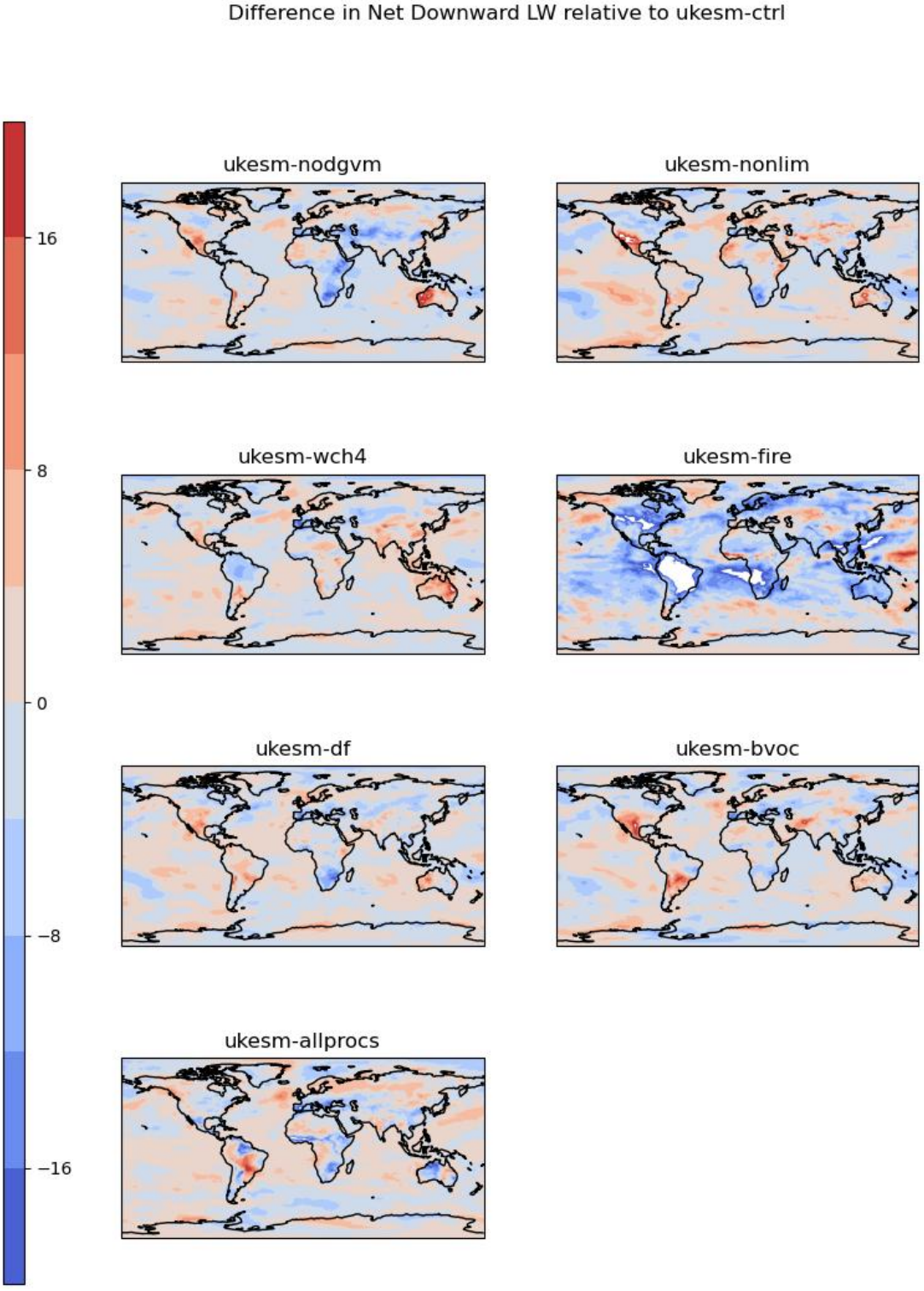

Figure S16: Difference in net downward longwave radiation (W/m2) relative to *ukesm-ctrl* for year 1990 of the 1pctCO2-cou simulation by each experimental configuration of UKESM1.1.

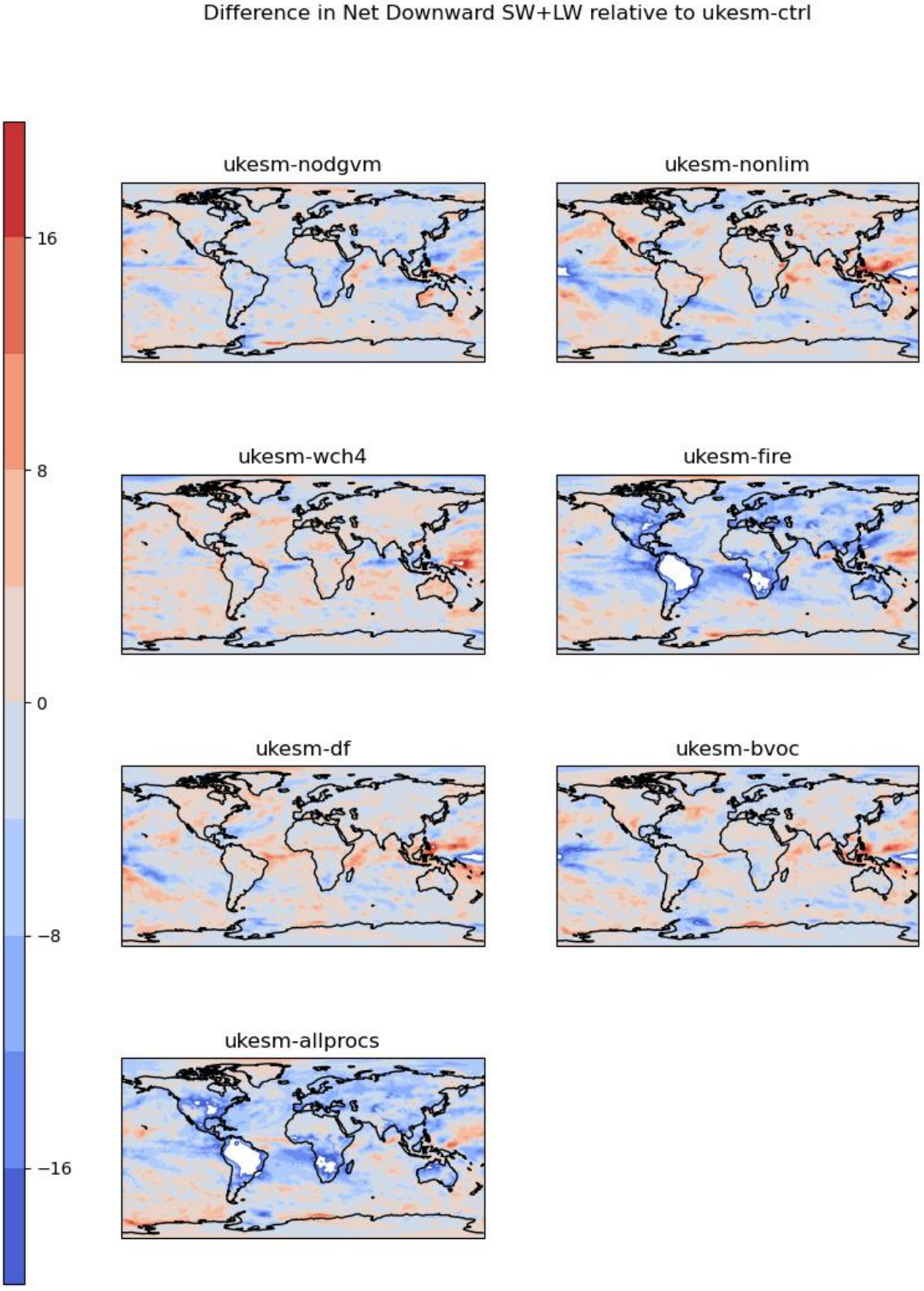

Figure S17: Difference in net downward shortwave plus longwave radiation (W/m2) relative to *ukesm-ctrl* for year 1990 of the 1pctCO2-cou simulation by each experimental configuration of UKESM1.1.

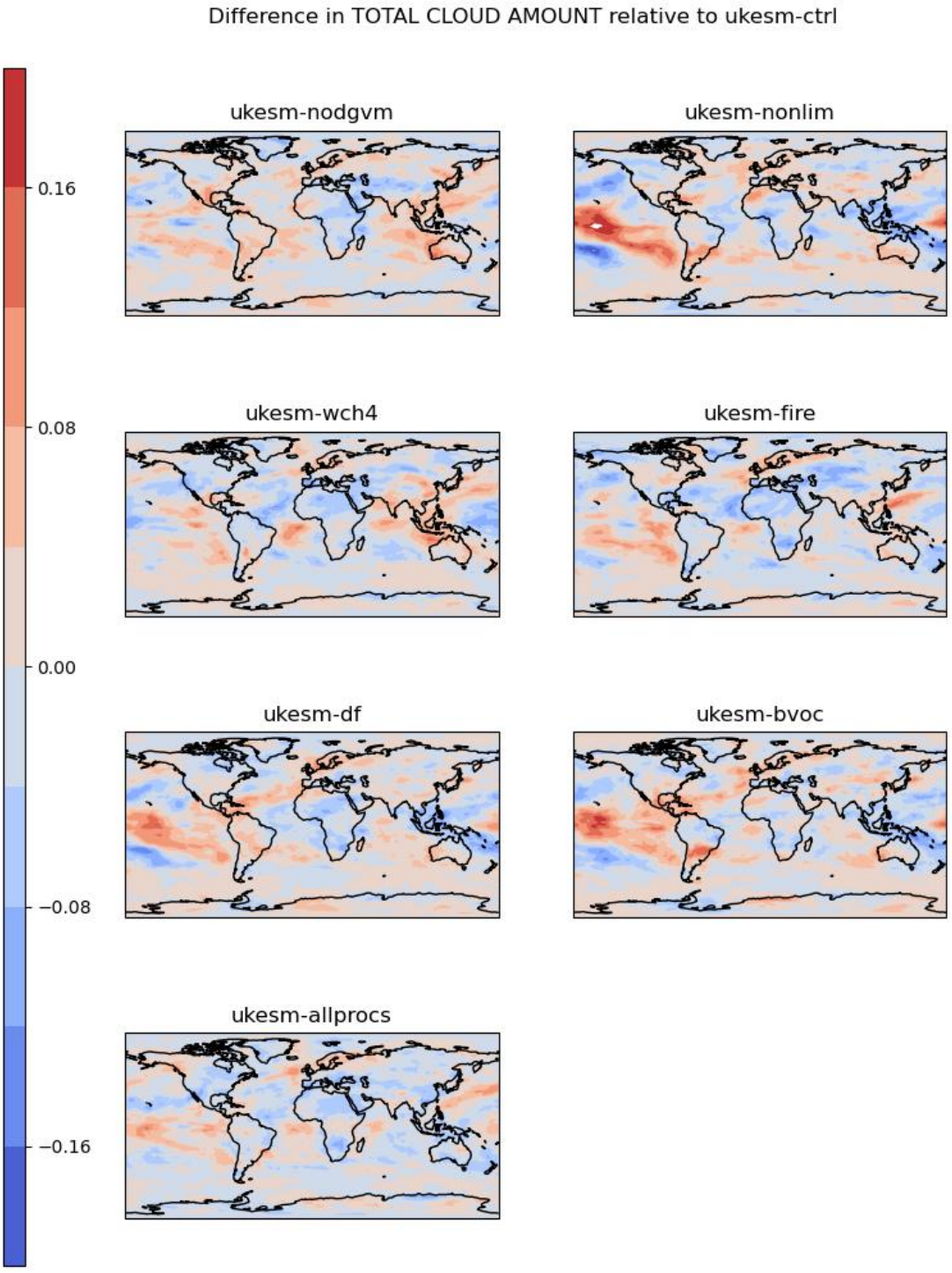

Figure S18: Difference in total cloud amount relative to *ukesm-ctrl* for year 1990 of the 1pctCO2-cou simulation by each experimental configuration of UKESM1.1.

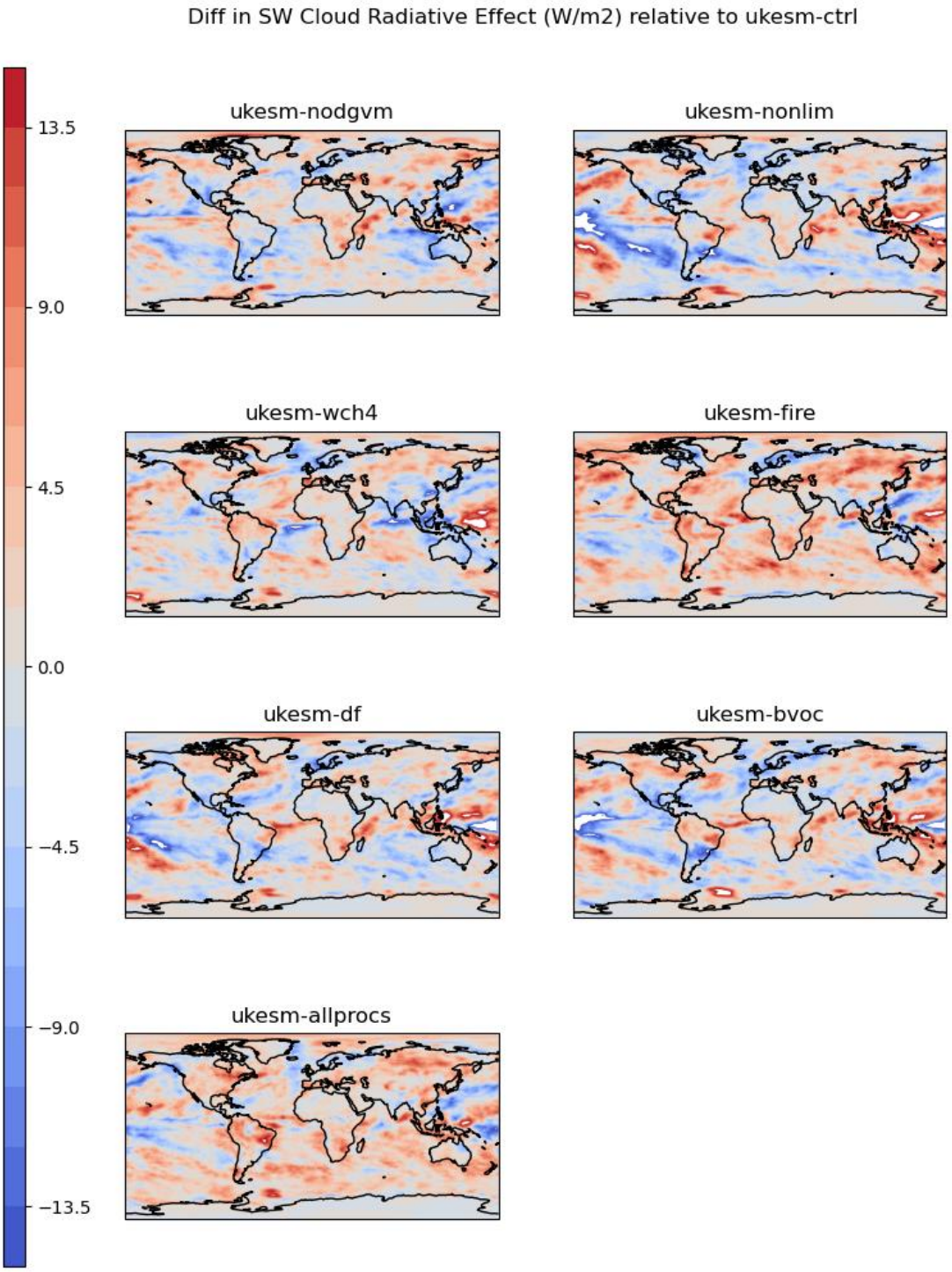

Figure S19: Difference in shortwave cloud radiative effect relative to *ukesm-ctrl* for year 1990 of the 1pctCO2-cou simulation by each experimental configuration of UKESM1.1.

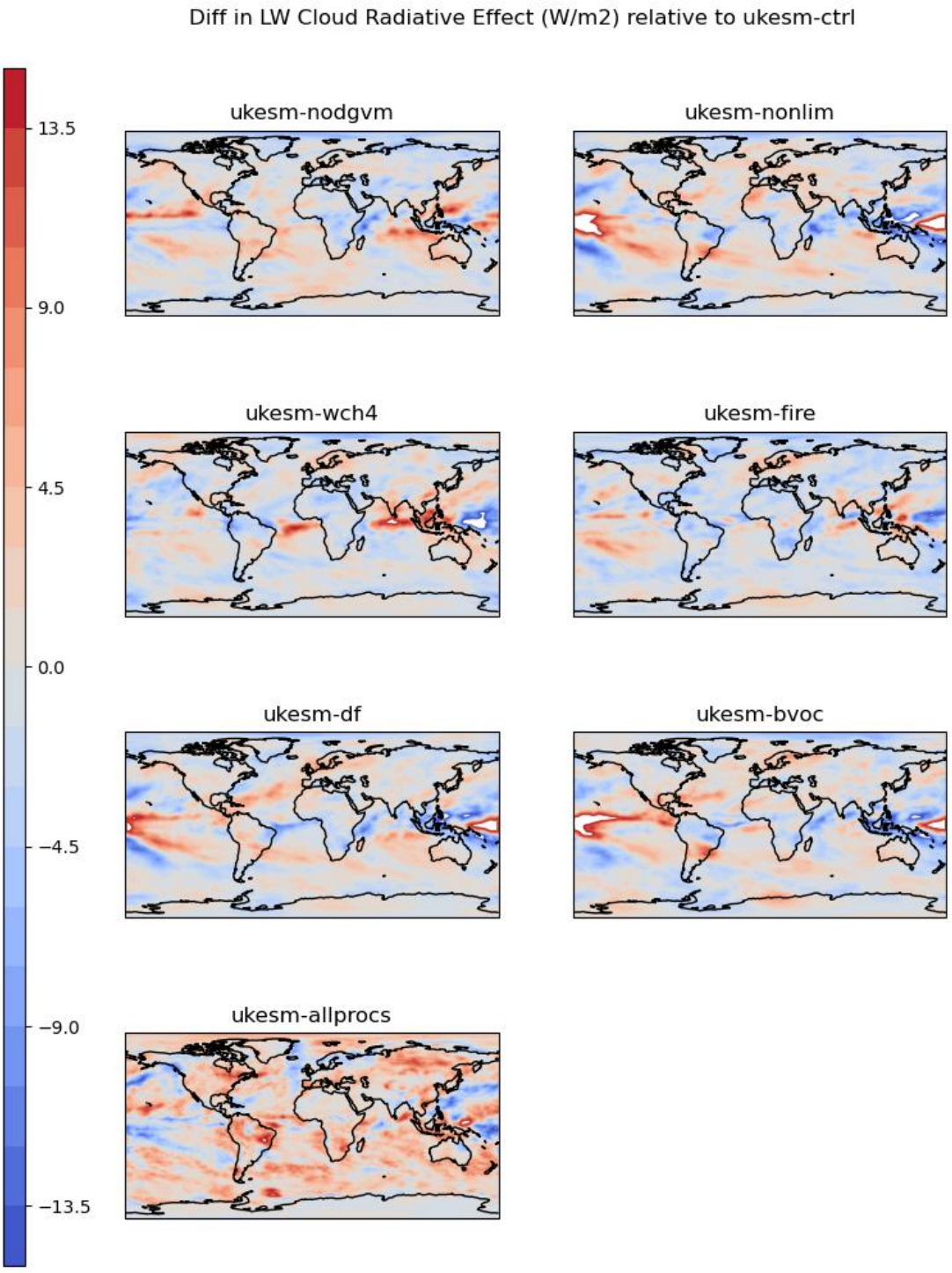

Figure S20: Difference in longwave cloud radiative effect relative to *ukesm-ctrl* for year 1990 of the 1pctCO2-cou simulation by each experimental configuration of UKESM1.1.

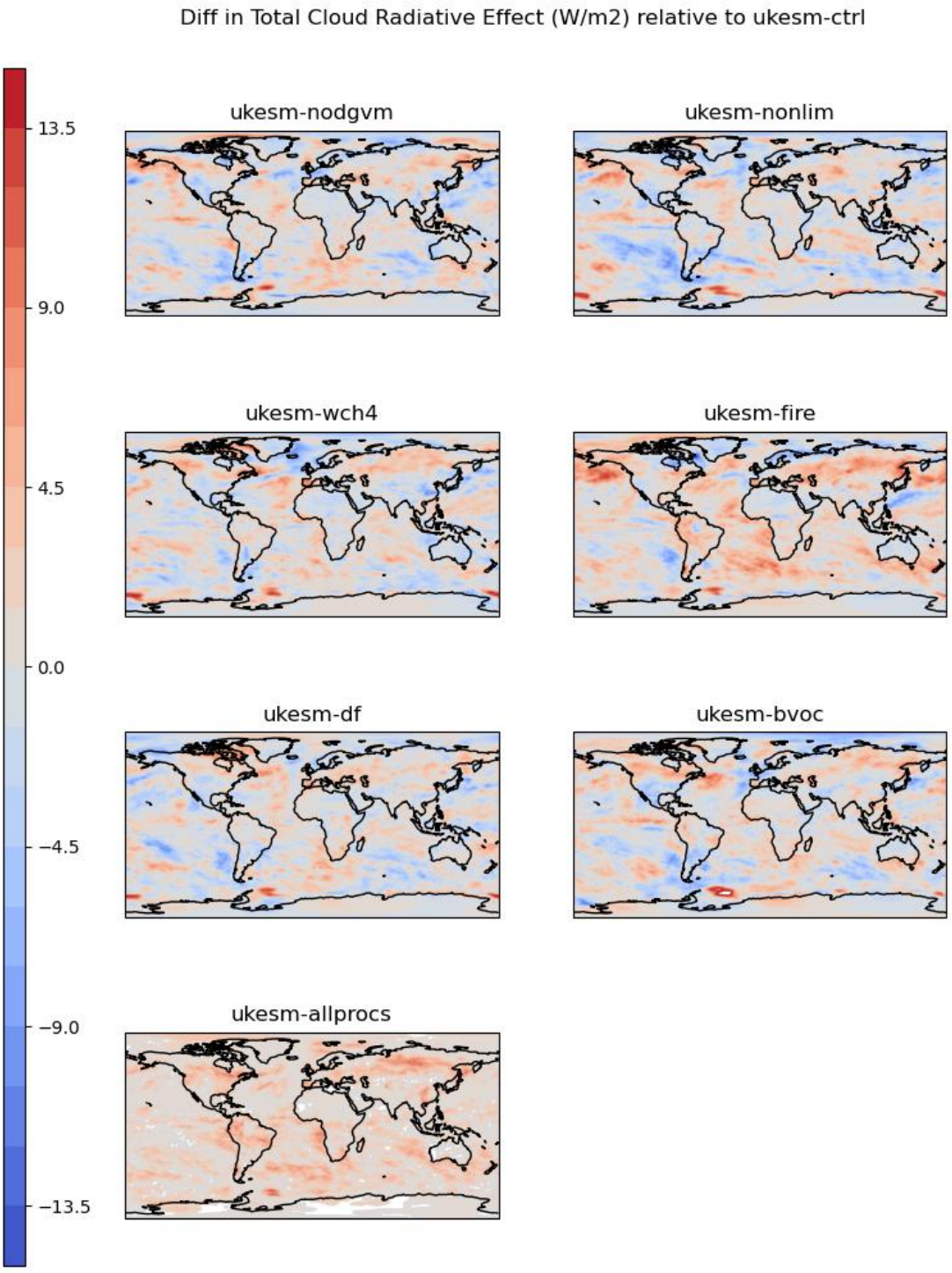

Figure S21: Difference in total (shortwave + longwave) cloud radiative effect relative to *ukesm-ctrl* for year 1990 of the 1pctCO2-cou simulation by each experimental configuration of UKESM1.1.